Civil Engineering and Applied Solutions

Research Article

journal homepage: ceas.journals.umz.ac.ir

CEAS Civil Engineering and Applied Solutions

Flood Hazard Assessment and Mitigation in the Tigris River: An HEC-RAS Approach (Al-Kut Dam to Al-Musandawq)

Mahmoud Mohammad Rezapour Tabari [a*], Milad Rahshabdiz [a], Mustafa Khudhair Tuama [a]

[a] *Department of Civil Engineering, Faculty of Engineering and Technology, University of Mazandaran, Mazandaran, Iran*

ARTICLE INFO

Article history:

Received 13 March 2026

Revised 31 March 2026

Accepted 01 June 2026

Available online 01 January 2027

Keywords:

Flood hazard management

HEC-RAS

Tigris river

Floods control

Flood wave routing

Hydraulic modeling

ABSTRACT

This study addresses the critical issue of flood hazard management in the Maysan region of Iraq, a city highly susceptible to recurrent and devastating floods, as tragically demonstrated by the 2019 flood event. Focusing on a 169 km reach of the Tigris River downstream of the Al-Kut barrage, including the Al-Musandawq channel, this research investigates the impact of riverine obstacles on flood dynamics. The primary objective is to assess and mitigate flood hazards through advanced hydrological modeling. The study employed the HEC-RAS model, utilizing 169 cross-sections surveyed in 2017 and incorporating digital elevation model (DEM) data. Model calibration, using hydrological and topographical inputs, yielded a Manning's roughness coefficient of 0.031 for the Tigris River and 0.028 for the Al-Musandawi channel. High accuracy was confirmed by Nash-Sutcliffe Efficiency (NSE) indices of 0.979 and 0.986, respectively, alongside other error metrics (RMSE, MAE). Model simulations revealed that flood waves were primarily delayed, reaching Maysan city with minimal dispersion, leading to inundation. To mitigate these risks, two management approaches were considered: (1) removal of islands and sidebars within the river reach, and (2) construction of a weir. Due to the high cost and limited effectiveness of removing natural obstacles, the focus shifted to structural solutions. Scenarios were developed to design a weir with an optimal crest elevation. The goal was to prevent downstream flow to Maysan city from exceeding 700 m^3s during flood seasons, while ensuring a minimum flow of 250 m^3s during dry seasons. Simulations of peak flow rates (4000, 2500, 1050, 533, and 250 m^3s) established an optimal weir crest elevation of 9.4 meters. This study provides crucial insights into flood mitigation strategies for the Tigris River, offering a data-driven approach to protect vulnerable downstream areas.

How to cite this article: Rezapour Tabari, M-M., Rahshabdiz, M., Khudhair Tuama, M. Flood Hazard Assessment and Mitigation in the Tigris River: An HEC-RAS Approach (Al-Kut dam to Al-Musandawq). Civil Engineering and Applied Solutions. 2027; 3(1): 98–116. doi:10.22080/ceas.2026.31452.1085

1. Introduction

Floods affect more people than any other natural disaster, killing more people each year, and climate change will exacerbate the problem of floods. Floods have an impact on the environment, social, and economic affairs [1]. Recurrent and high-magnitude flooding in agricultural areas poses a serious threat to crop productivity and food security, often resulting in substantial economic losses. This reality underscores the necessity of systematic flood analysis, not only to enhance our understanding of flood behavior but also to inform the development of effective and context-specific flood mitigation strategies. Although direct, in situ flood observations provide invaluable insights, their acquisition is frequently constrained by logistical, temporal, and safety limitations, highlighting the need for complementary analytical and modeling approaches.

* Corresponding author.
E-mail addresses: mrtabari@umz.ac.ir (M. Mohammad Rezapour Tabari).

https://doi.org/10.22080/ceas.2026.31452.1085
ISSN: 3092-7749/

2. Literature review

In the Middle East, the continued and widespread use of the HEC-RAS model is largely driven by the limited availability and reliability of high-resolution elevation data. Studies conducted along the Tigris River clearly illustrate this constraint. For instance, Mohammed Ali and Khairallah, despite having access to only four years of discharge records, successfully identified flood-prone streets in the city of Tikrit with notable spatial accuracy [2]. Similarly, the study by Sabeeh and Alabdraba demonstrated that minor adjustments to the Manning roughness coefficient were sufficient to achieve a close agreement between simulated water levels and observed gauge data [3]. These outcomes highlight not only the robustness of HEC-RAS under data-scarce conditions, but also its practical value in regions where field measurements and detailed topographic datasets are difficult to obtain.

At the global scale, however, a contrasting pattern emerges. By systematically analyzing three decades of Landsat imagery, Pekel and colleagues documented a net loss of approximately 90,000 square miles of permanent lakes and river surfaces worldwide, while simultaneously noting the expansion of artificial water bodies, largely driven by dam construction across Asia [4, 5]. Complementing this physical perspective, Sullivan et al. employed nighttime light data as a proxy for human settlement and revealed a marked demographic shift toward areas classified as low flood risk, where the proportion of residents increased from 8 to 11% within a 15-year period [6]. Importantly, this change reflects patterns of human relocation and land-use decisions rather than any abrupt intensification of rainfall regimes, underscoring the growing role of socio-economic dynamics in reshaping global flood exposure.

Some researchers now combine conventional hydrological models with machine learning to provide very good predictions of extreme flooding in ungauged areas [7]. In the Kerala floods of 2018, Suresh and his team monitored the dams from satellites and proved that if the dam operators had opened the gates two days earlier, half of the disaster would not have occurred [8].

Coastal municipalities face a particularly precarious trajectory. A comprehensive systematic review by Aziz et al. [9] underscores a global systemic lag: the rate of urban expansion in nearly all major coastal hubs is currently outstripping the deployment of flood-defense infrastructure. While robust decision-support frameworks are theoretically available [10, 11], their practical integration into urban governance remains alarmingly deficient. This misalignment is starkly evident in the United States; Hino et al. [12] demonstrated that in regions like North Carolina, the continued authorization of floodplain construction has caused the inherent risk profile to escalate at a pace far exceeding eustatic sea-level rise. A parallel socio-spatial inequity is documented in the Canadian context, where Chakraborty et al. [13] identified a troubling correlation between socio-economic vulnerability and proximity to high-risk riparian zones.

Within the African context, the adoption of Nature-Based Solutions (NBS) has gained significant empirical support. Research conducted by Jemberie and Melesse [14] in Addis Ababa, complemented by the modeling efforts of Long'or Lokidor et al. [15] in East Africa, demonstrates that decentralized interventions, specifically retention ponds, permeable sewerage systems, and vegetative roofing, can substantially attenuate peak runoff. However, these studies converge on a critical socio-political caveat: the hydrological efficacy of such green infrastructure is fundamentally contingent upon robust municipal oversight and the stringent enforcement of building codes by local authorities.

While satellite imagery is a popular tool for flood mapping, its utility is frequently hampered during actual flood events by persistent cloud cover, rendering the acquired data unusable [16]. Consequently, observation-based maps, though valuable for documenting specific occurrences, are insufficient for predictive purposes, such as forecasting extreme events or evaluating the efficacy of engineered flood defenses like levees. This underscores the indispensable role of numerical hydrological models. These models enable scenario analyses by allowing for the simulation of various hydrological conditions, including altered precipitation regimes, land-use changes, and dam operational strategies, to predict their respective impacts. Widely adopted tools, such as HEC-RAS developed by the U.S. Army Corps of Engineers, have become de facto industry standards due to their robust computational capabilities, user-friendly interfaces, and, critically, their open-source accessibility [17]. Researchers leverage these platforms for diverse applications: generating flood risk maps for urban planning, reconstructing past flood events to identify causal factors and system failures, and pre-emptively assessing mitigation strategies before substantial capital investment in physical infrastructure [18, 19]. The ongoing development and updates by the Corps ensure the continued relevance and accuracy of HEC-RAS, maintaining its utility for predictive flood management over extended periods.

In summary, while the technical repertoire for flood mitigation, ranging from advanced numerical modeling and satellite-based monitoring to cost-effective green infrastructure, is already well-established, the primary impediment to effective flood management is no longer a deficit in technological expertise, but rather a crisis of political agency and the prioritization of short-term economic gains over the protection of socio-economically vulnerable populations. Flood hazards pose a significant and growing threat to populations and infrastructure worldwide, exacerbated by climate change and increasing urbanization. The Tigris River basin, a vital water resource for Iraq, is particularly susceptible to severe flood events. While historical flood management efforts have been undertaken, the dynamic interplay between river discharge, channel morphology, and the capacity of escape routes, especially in densely populated areas like the region surrounding Amarah, remains inadequately understood. Previous studies in the Tigris basin have often relied on simplified one-dimensional (1D) hydraulic models, limited spatial data resolution, or did not comprehensively evaluate integrated flood mitigation strategies, hindering the accurate prediction of flood inundation extent and the effective assessment of management interventions. This study aims to bridge this knowledge gap by employing a state-of-the-art integrated 1D–2D HEC-RAS model. We focus on a critical 169-km reach of the Tigris River between the Kut and Al-Musandawq dams, a stretch characterized by increasing alluvial formations and dikes that have significantly compromised the flow gradient. Utilizing HEC-RAS for one- and two-dimensional hydraulic modeling, we assess this critical reach. Historical data underscores a dramatic

hydrological shift: peak discharge at the Kut Dam has plummeted from 3,000 m³/s in 1988 to a mere 200 m³/s by 2010. Despite this reduction in baseflow, the region remains susceptible to catastrophic flooding, as evidenced by major events in 1950, 1957, and 1988, as well as more recent inundations in 2013 and 2019. Our research addresses the following: (1) developing and calibrating a high-resolution coupled 1D–2D model for this complex reach; (2) quantitatively assessing the effectiveness of two distinct flood mitigation scenarios, natural modification (island removal) and structural control (submerged weir); and (3) determining the optimal design parameters for the most promising mitigation measure. By providing a detailed, data-driven analysis, this work offers crucial insights for enhancing flood resilience and informing sustainable water management practices in the Tigris River basin.

3. Methodology

3.1. Study area

The study reach encompasses approximately 87 kilometers along the Tigris River, situated within the Wasit Governorate of central Iraq (Fig. 1). This segment extends from the immediate upstream vicinity of the Kut Dam (32°30'N, 45°50'E) to its terminus at the Al-Musandawq spillway (32°15'N, 46°15'E). Geomorphologically, the area is positioned within the heart of the historic Mesopotamian floodplain, a region defined by the convergence of the Tigris and Euphrates hydrological systems. The study area is bounded by latitudes 32.10–32.40°N and longitudes 45.40–46.30°E. The regional climate is characterized as semi-arid, experiencing extreme thermal peaks during the summer months and temperate winters. Precipitation is notably limited, with average annual rainfall ranging between 150 and 200 mm.

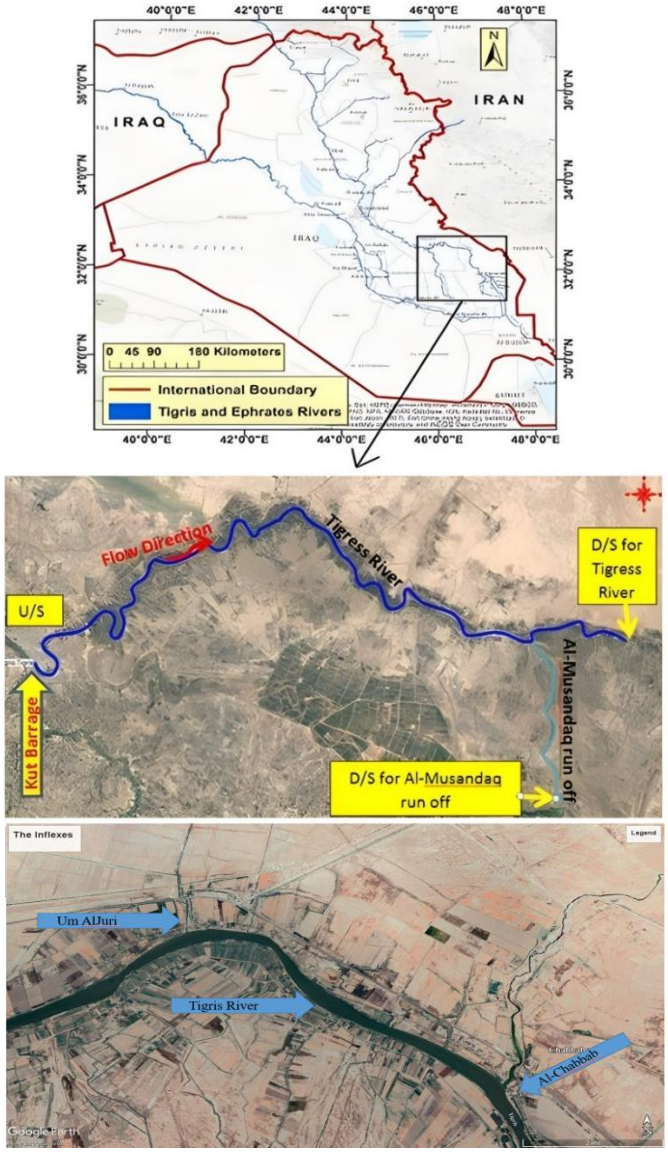

Fig. 1. Geographical location of the study area along the Tigris River reach.

In this reach, the Tigris River exhibits a high degree of sinuosity, confined by prominent natural levees that rise to 20 meters above the surrounding floodplain. These elevated alluvial features have historically facilitated productive irrigated agriculture and supported dense riparian ecosystems, which serve as the socio-economic backbone of the region. The longitudinal profile of the river shows a progressive decrease in hydraulic gradient; while the slope is approximately 4 cm/km near the Kut Dam, it attenuates significantly further downstream. This reduction in flow velocity encourages substantial sediment deposition and enhances the floodplain's natural capacity for flood attenuation, effectively functioning as a vast hydrological buffer during high-discharge events.

A central feature of the regional flood-control infrastructure is the Al-Musandawq escape channel (Fig. 2), a major regulated spillway situated on the right bank of the Tigris. Spanning approximately 400 m at its confluence with the main river, this strategic diversion was engineered to mitigate catastrophic flood risks by rerouting surplus discharge into adjacent topographic depressions. The facility's hydraulic significance was most notably demonstrated during the historic flood of 1974, when it successfully diverted a peak flow of 1,800 cubic feet per second, thereby safeguarding downstream agricultural lands and primary irrigation canals. To this day, the spillway remains under the operational jurisdiction of the Ministry of Water Resources, serving as a critical safeguard for the basin's hydraulic stability.

Fig. 2. Flood-control infrastructure in the Al-Musandawq channel.

3.2. Study approach

At the initial stage, the hydraulic model is calibrated using the 2019 flood event to reproduce the observed flood dynamics and to quantify its impacts along the selected reach of the Tigris River, extending from downstream of Kut Barrage to the outlet of the Al-Musandawq channel. To support this calibration and ensure hydraulic realism, the study begins with a systematic identification and characterization of flood-prone reaches through field visits along the river corridor, where historically inundated and high-risk areas were documented. In parallel, long-term hydrological records and flood event statistics were compiled to obtain the flood discharge time series required for modeling.

Alongside the hydrological dataset, the hydraulic geometry of the river in the selected cross-sections was extracted using available topographic information, with DEM maps playing a key role in determining the channel-bed characteristics and the overall topography of the flow path. Based on a detailed review of the river's cross-sections, the geometric dataset was refined by identifying locations with noticeable changes in hydraulic behavior (e.g., significant variations in flow velocity and cross-sectional form). Accordingly, additional cross-sections were introduced in reaches exhibiting hydraulic complexity to improve the representativeness of the model geometry.

Using the compiled and refined hydrological and topographic inputs, the HEC-RAS model was developed under both steady and unsteady flow conditions. Key model parameters, particularly Manning's roughness coefficient, were calibrated using the 2019 flood discharge time series. Model calibration aimed to reproduce observed flood behavior with acceptable accuracy, and performance was evaluated using standard hydraulic modeling metrics and comparisons between simulated water levels and observed flood characteristics along the study reach.

Following calibration, two alternative flood management strategies were systematically examined to identify the most efficient approach for mitigating flood risk in the study area. The first strategy investigates the hydraulic implications of removing riverine islands from the Tigris River channel. This scenario evaluates whether the flood wave can be conveyed safely at lower water levels than those currently experienced. To implement this intervention, cross-sections containing islands were modified accordingly, and the model was rerun using the 2019 flood hydrograph. The resulting water levels and flow characteristics were then compared with observed flood data to assess the effectiveness of island removal.

The second strategy considers the implementation of a hydraulic control structure in the form of a submerged weir installed upstream of the Al-Musandawq channel bifurcation. The crest elevation of the weir was optimized at 9.406 m to enable controlled diversion of surplus floodwater toward the Al-Musandawq channel. During flood conditions, the structure limits the discharge directed toward Amarah City to a maximum of 700 m^3/s, while efficiently routing excess flows away from the urban reach. Conversely, during low-flow periods when the Tigris River discharge falls below 250 m^3/s, the flow configuration preferentially directs the available discharge toward Amarah City, with negligible or no diversion to the Al-Musandawq channel. The overall methodological framework adopted in this study is summarized in the flowchart presented in Fig. 3.

Fig. 3. Structure of the proposed approach to flood management.

3.2.1. Mathematical modeling of unsteady open-channel flow

The fundamental governing equations for one-dimensional (1D) and two-dimensional (2D) unsteady flow are first introduced. Alongside the full formulations, simplified forms of these equations are presented, accompanied by a concise explanation of their mathematical solution procedures. To enhance understanding, the discussion is supplemented with illustrative examples that demonstrate practical applications of the governing principles. In turbulent open-channel flows, both spatial and temporal variations play a significant role in defining the flow behavior. Under such conditions, the mass conservation and momentum provide the most reliable framework for describing flow dynamics. The Shallow Water Equations, commonly referred to as the Saint-Venant equations, offer an accurate representation of flow processes when these conservation laws are satisfied.

The solutions to these governing equations are presented for both one-dimensional and two-dimensional cases. The following section focuses on unsteady one-dimensional flow, beginning with the formulation of the one-dimensional continuity equation.

3.2.2. The two-dimensional unsteady flow

The one-dimensional continuity equation (Eq. 1):

$$\frac{\delta A}{\delta T} + \frac{\delta Q}{\delta x} = q \tag{1}$$

where, A indicates the cross-section (m^2), Q represents the flow in cross-section (m^3/s), x shows the distance along the channel (m) and q is the lateral inflow (m^2/s).

The one-dimensional momentum equation (Eq. 2):

$$\frac{\delta Q}{\delta t} + \frac{\delta VQ}{\delta X} + gA\left(\frac{\delta z}{\delta x} + S_o + S_f\right) = 0 \tag{2}$$

where, V denotes the flow velocity (m/s), g represents the gravitational acceleration (m/s^2), z is the water depth (m), S_0 is the channel bed slope, S_f denotes the friction slope, and t represents time (s).

3.2.3. The two-dimensional unsteady flow

The two-dimensional continuity equation (Eq. 3):

$$\frac{\partial H}{\partial t} + \frac{\partial (hu)}{\partial x} + \frac{\partial (hv)}{\partial y} + q = 0 \quad (3)$$

where, g is the gravitational acceleration, u denotes the flow velocity in the x-direction, and R is the hydraulic radius. In addition, H represents the water surface elevation, h is the water depth, u and v are the depth-averaged velocity components in the x- and y-directions, respectively, and q is the source term accounting for external inflows, such as precipitation and lateral contributions from surrounding areas [20].

The two-dimensional momentum equation (Eqs. 4 and 5):

$$\frac{\partial u}{\partial t} + u\frac{\partial u}{\partial x} + v\frac{\partial u}{\partial y} = -g\frac{\partial H}{\partial x} + \nu_t\left(\frac{\partial^2 u}{\partial_y^2}\right) - c_f u + f_v \quad (4)$$

$$\frac{\partial v}{\partial t} + u\frac{\partial v}{\partial x} + v\frac{\partial v}{\partial y} = -g\frac{\partial H}{\partial y} + \nu_t\left(\frac{\partial^2 v}{\partial x^2} + \frac{\partial^2 v}{\partial y^2}\right) - c_f v + f_u \quad (5)$$

where, ν_t is the eddy viscosity coefficient, c_f represents the bed friction coefficient, f is the Coriolis parameter [21]. The first term corresponds to convective acceleration, while the subsequent terms account for the forces induced by gravity, turbulent diffusion, bed friction, and the Coriolis effect. By applying Manning's formulation, the friction coefficient c_f in the x-direction can be expressed as follows (Eq. 6):

$$c_f = \frac{n^2 g|u|}{R^{4/3}} \quad (6)$$

Where, n denotes Manning's roughness coefficient.

3.2.4. Modeling simplifications

To improve computational efficiency and minimize the risk of numerical instability, the full Shallow Water Equations are commonly simplified by neglecting selected terms in the momentum equations. Such simplifications are most frequently adopted in two-dimensional modeling frameworks, where reducing computational complexity is essential for achieving stable and practical simulations.

3.2.5. Diffusive wave approximation

When gravity and friction are assumed to be the dominant forces acting on the control volume, the momentum equation can be simplified to the diffusive wave approximation. This assumption is based on the premise that these forces exert the greatest influence on the flow dynamics under the conditions considered.

$$g\nabla H = -c_f V \quad (7)$$

where, V denotes the flow velocity vector, expressed as $\mathrm{V} = (u, v)$ and ∇ denotes the differential operator. When bottom friction is evaluated using Manning's formulation, Eq. 7 can be rewritten as:

$$V = \frac{-(R(H))^{\frac{2}{3}}}{n} \quad (8)$$

where, $R(H)$ represents the hydraulic radius corresponding to the water surface elevation H, Substituting Eq. 8 into the continuity equation (Eq. 3) and expressing the result in vector form yields the following expression (Eqs. 9 and 10):

$$\frac{\partial H}{\partial t} + \nabla\beta\nabla H + q = 0 \quad (9)$$

where,

$$\beta = \frac{-(R(H))^{\frac{2}{3}}}{n} \quad (10)$$

By applying the diffusive wave approximation to the Shallow Water Equations, the governing equations for two-dimensional flow (Eqs. 3, 4, and 5) can be simplified to the form presented in Eq. 9. This approximation reduces computational time and can improve numerical stability. It is particularly suitable for representing flow variations in moderately steep to steep channel reaches. However, it does not capture flow separation, eddies, or momentum transfer effects [22].

3.2.6. Solving techniques

The Shallow Water Equations constitute a set of partial differential equations that cannot be solved analytically. To obtain numerical solutions for the flow variables, these equations must be integrated using appropriate numerical methods. Both the water surface elevation and the flow velocity vary continuously in space and time, and at each computational time step, the model must determine the values of these variables across the entire domain. Numerical schemes typically impose constraints on the Courant

number to ensure solution accuracy and stability. The Courant number can be calculated using Eq. 11:

$$C = \frac{V\Delta t}{\Delta x} \tag{11}$$

where, Δt is the computational time step, and Δx represents the spatial discretization- corresponding to cross-section spacing in one-dimensional models and cell size in two-dimensional models.

The unsteady flow component of the model incorporates a variety of advanced features, including automatic calibration, user-defined rules, hybrid one-dimensional and two-dimensional unsteady flow modeling, dam-break analysis, levee overtopping and failure, pumping station operation, navigation dam management, and pressurized pipe systems, among others. These functionalities are accessible under the "unsteady flow" module and collectively enhance the model's ability to represent complex hydraulic and hydrologic processes while preserving the real-world characteristics of the study area.

In this study, Manning's roughness coefficient (n) was assigned based on standard references, including Chow, Maidment and Mays [23] This coefficient quantifies the resistance to flow and is critical for accurately simulating channel hydraulics. The computational grid consists of cells, with flow interactions occurring across cell faces, which act as the interfaces between adjacent elements. A 100 m × 100 m square cell grid was employed, with the cells oriented at various angles to accommodate the river geometry.

The governing equations were solved using a stepwise finite-volume approach, which estimates mean flow quantities by integrating over each reference volume. This methodology allows for flexible handling of unstructured grids and complex channel geometries. Subsequently, elevation–volume relationships were computed for each cell, followed by derivation of hydraulic properties such as wetted perimeter and cross-sectional area, using procedures analogous to those applied in one-dimensional preprocessing.

River calibration was performed by adjusting Manning's roughness coefficient along the reach to match observed flow rates and water levels. HEC-RAS was used to simulate these hydraulic variables. Conceptually, calibration can be viewed as an inverse problem, in which initial and local parameters of the system are estimated by comparing model outputs to observed data. During this process, the objective function (error index) is minimized by iteratively updating parameter values within defined ranges, ensuring that the model accurately reproduces the observed flow behavior along the study reach. In this section, the mathematical formulations of the error indicators employed during the model calibration process are presented in the form of Eqs. 12-14.

- **Root Mean Square Error (RMSE)**

The Root Mean Square Error (RMSE) provides a measure of the average magnitude of errors between observed and simulated values, giving higher weight to larger deviations. It is defined as:

$$RMSE = \sqrt{\frac{\sum_{i=1}^{N}(o_i - o_f)^2}{N}} \tag{12}$$

where, N is the total number of observations, o_i is the observed value, and o_f is the simulated value.

RMSE values range from 0 to infinity, with lower values indicating better model performance and a value of zero representing a perfect match between observations and simulations.

- **Nash–Sutcliffe Efficiency (NSE)**

The Nash–Sutcliffe Efficiency (NSE) evaluates the predictive skill of the model relative to the variance of the observed data. It is expressed as:

$$NSE = 1 - \frac{\sum_{i=1}^{N}\left(o_i - o_f\right)^2}{\sum_{i=1}^{N}(o_i - \bar{o})^2} = 1 - \left(\frac{RMSE}{SD}\right) \tag{13}$$

where, $\bar{O}$ is the mean of observed values, SD is the standard deviation of the observations. NSE values range from $-\infty$ to 1. A value of 1 indicates a perfect agreement between observed and simulated values, while values below zero suggest that the model performs worse than using the mean of observations as a predictor. An NSE value above 0.75 is considered acceptable, and above 0.90 is deemed excellent for hydrodynamic models.

- **Mean Absolute Error (MAE)**

The Mean Absolute Error (MAE) provides the average magnitude of errors in absolute terms, without considering their direction. It is calculated as:

$$MAE = \frac{1}{n}\sum_{i}^{n} =_1 |o_i - \bar{o}| \tag{14}$$

MAE is a non-negative metric with no theoretical upper limit. A value of zero corresponds to a perfect simulation, with increasing values indicating larger deviations between observed and predicted data.

3.3. Hydraulic modeling using HEC-RAS

3.3.1. Input data

The geometric framework of the investigated reach was constructed by integrating high-resolution spatial data into the HEC-RAS environment. This setup involved the parameterization of a Digital Elevation Model (DEM), the definition of representative cross-sections along the 87-km segment, and the establishment of hydraulic boundary conditions. The core components of the model geometry are synthesized below:

a) Digital elevation model (DEM)

The topographic foundation of the hydraulic model was established using a Digital Elevation Model (DEM), which provides a high-fidelity three-dimensional representation of the terrain. For the Tigris River basin, where topographical accuracy is paramount for flood routing, SRTM (Shuttle Radar Topography Mission) data was utilized. Over the last decade, SRTM has become a benchmark in global hydrological studies due to its consistent homogeneity and proven accuracy relative to other open-source datasets. In this study, the SRTM-derived DEM was instrumental in delineating the floodplain's geomorphological features and extracting the precise elevation profiles required for the 1D and 2D hydraulic simulations.

b) Cross-section

Bathymetric data for the Tigris River were obtained from the Department of Irrigation in Kut. This dataset, comprising detailed cross-sectional profiles from the downstream of the Kut Dam to the Al-Musandawq escape channel, was provided in tabular format. These profiles were subsequently integrated into the HEC-RAS modeling environment, where the river's geometry was meticulously reconstructed within the geometric editor to ensure a high-fidelity representation of the channel morphology.

c) Interpolation of the Cross-section

To enhance the numerical stability of the hydraulic simulation and ensure a refined representation of the river's profile, additional cross-sections were generated via interpolation between the field-surveyed stations (Table 1). This procedure is essential in reaches where significant fluctuations in velocity head occur, as abrupt changes can impede the accurate calculation of the energy gradient. By establishing uniform computational intervals through interpolation, the model more effectively captures the transition of flow energy and reduces potential convergence errors.

Table 1. Comparative analysis of cross-sectional profiles between the geometric data editor and ras mapper for a 21-km segment of the Al-Musandawq reach (starting at sta. 0+000).

Cross-section station (From Downstream to Upstream)	Elevation in Geometry Edit	Elevation in the RasMapper	Difference
21+000	4.7	7	-2.3
20+000	10.53	8	2.53
19+000	10.48	8	2.48
18+000	10.24	6.534	3.706
17+000	10.3	7	3.3
16+000	9.86	7	2.86
15+000	9.82	7	2.82
14+000	9.58	8	1.58
13+000	9.54	7.832	1.708
12+000	7.3	8	-0.7
11+000	8	7.83	0.17
10+000	8	8	0
9+000	9	7.241	1.759
8+000	9	8	1
7+000	9	8.438	1.438
6+000	9.62	8	1.62
5+000	10	7.98	2.02
4+000	9.98	7.563	2.417
3+000	9.66	7	2.66
2+000	9.5	8	1.5
1+000	10	8.85	1.15
0+000	10	9	1

d) Boundary conditions(unsteady flow data)

Boundary conditions are critical parameters for linking one- and two-dimensional flow areas within the HEC-RAS environment.

In this study, the hydraulic regime was driven by three specific flow hydrographs, derived from hydrological data provided by the Al-Kut Water Resources Division for the high-flow period of April 2019. The primary upstream boundary condition was defined by the main Tigris flow hydrograph. To ensure a comprehensive water balance within the reach, two additional lateral inflow hydrographs were integrated to account for the contributions of the Um Aljury and Al-Chabab tributaries. This configuration allows the model to accurately simulate the interaction between the main channel and its secondary inflows during peak discharge events.

e) Development of the Integrated 1D-2D Hydrodynamic Model

Within the HEC-RAS modeling framework, the unsteady flow module provides a flexible environment for representing flow dynamics across complex river systems. This component allows one-dimensional, two-dimensional, and coupled one–two-dimensional simulations within interconnected networks of open channels, floodplains, and alluvial fans. It is designed to accommodate a wide range of flow conditions, enabling the analysis of subcritical, supercritical, and transitional regimes, including hydraulic jumps and drawdown processes, as they evolve over time. A key strength of this module lies in its seamless integration of hydraulic computations previously developed for steady-flow conditions. Calculations associated with cross-sections, bridges, culverts, and other hydraulic structures are directly embedded in the unsteady-flow framework, ensuring consistency in the representation of channel geometry and structural controls. In addition, the module offers advanced functionalities such as dam-break and levee-breach simulations, overtopping analysis, pumping station operations, navigation dam controls, and pressurized pipe systems. The inclusion of automated calibration options, user-defined operational rules, and the ability to combine one- and two-dimensional domains further enhances its applicability for realistic and site-specific flood modeling studies.

f) One-Dimensional Hydraulic Modeling Using HEC-RAS

Hydraulic modeling in the HEC-RAS environment begins with a structured data preparation stage, in which real-world terrain and river features are translated into a computational framework through GIS-based processing. During this stage, spatial registration and georeferencing are applied to ensure that all geometric elements accurately reflect their physical location and scale. This workflow facilitates efficient data organization and calibration, while maintaining the essential spatial characteristics of the study area. In the present study, all spatial analyses and data integration tasks were carried out using the RAS Mapper module in HEC-RAS version 5.0.7.

Following data preparation, the model was populated with the required geometric and hydraulic inputs. These included a digital elevation model (DEM) representing watershed topography, detailed river cross-section geometries, and Manning's roughness coefficients assigned separately to the main channel and adjacent floodplains. Cross-sections derived from the DEM, supplemented by available field survey data, formed the core geometric basis of the hydraulic model. Within the Geometry Editor, the river system was defined by sequentially connecting 126 cross-sections from upstream to downstream, thereby establishing a continuous representation of flow conveyance along the modeled reach.

g) Calibration of the HEC-RAS model

In river hydraulic simulations, Manning's roughness coefficient is widely recognized as the most sensitive parameter influencing flow resistance and water-level predictions. Model calibration is therefore performed by systematically comparing simulated outputs with field observations collected at corresponding locations and iteratively adjusting the roughness coefficient (n) to achieve the closest possible agreement. In this study, calibration was undertaken along the entire modeled reach by simulating observed discharges and flow depths using the HEC-RAS framework and refining the overall resistance represented by Manning's n.

From a methodological perspective, calibration constitutes an inverse problem, as it seeks to infer representative initial and spatially distributed parameters of the river system based on a limited set of observed hydraulic variables. Traditionally, hydrodynamic models have relied on manual calibration, in which parameter values are progressively modified to reduce discrepancies between modeled and measured data. This process effectively minimizes an objective function by adjusting parameter sets within physically reasonable ranges, thereby ensuring that the calibrated model remains consistent with the hydraulic behavior of the river under the prevailing flow conditions, as described below.

h) Output of HEC-RAS

The graphical and reporting modules provide a comprehensive set of visualization tools for interpreting model outputs. These tools generate x–y plots representing the river schematic, cross-sectional geometry, longitudinal water-surface profiles, rating curves, hydrographs, and a range of additional hydraulic variables. Such visual outputs play a key role in diagnosing model behavior, evaluating simulation performance, and effectively communicating hydraulic responses under different flow conditions.

3.3.2. Flood control methods

Flood control strategies are implemented to reduce or eliminate the damaging consequences of floodwaters on human settlements and infrastructure. Such strategies range from long-established practices, such as the use of vegetation to enhance water retention, hillside terracing to slow surface runoff, and the construction of diversion channels to redirect excess flows, to engineered interventions including embankments, artificial lakes, dams, reservoirs, and retention basins designed to temporarily store floodwater during extreme events. In the context of the present study, expert consultations with engineers responsible for the Kut Dam and the Al-Architecture Dam, combined with field observations and measurements obtained during the 2019 flood event, were used to estimate the maximum discharge that can be safely conveyed through the modeled river reach. This threshold was determined to be approximately 700 m^3/s. Building on this constraint, the objective of this research is to identify an optimal flood management

approach capable of protecting downstream urban areas along the Tigris River, particularly in the vicinity of the Al-Musandawq channel branching, from future flood hazards.

4. Results and discussion

4.1. HEC-RAS Model calibration and verification

Along a river reach, Manning's roughness coefficient can vary downstream due to changes in channel and floodplain characteristics. Factors influencing n include bed and bank surface texture, vegetation, water stage, discharge, and channel irregularities. In general, n may be relatively high during high-stage flows in rocky or vegetated sections, whereas in most cases, the coefficient tends to decrease as discharge increases. In this study, calibration of the global Manning's n values formed a key part of the model validation strategy. The calibration process was carried out using observed data from April 2019. Based on iterative model runs, Manning's n values were systematically adjusted within physically plausible ranges: 0.021 to 0.037 for the Tigris river and 0.020 to 0.028 for the Al-Musandawq channel. These ranges are based on established literature values for similar riverine and engineered channel conditions (e.g., Chow [24]) and preliminary field observations. These calibrated values are summarized in Table 2. The verification of the unsteady flow model was performed by comparing simulated discharges against measured values. This comparison, illustrated in Fig. 4, demonstrates the model's ability to reproduce the observed variability in flow along the study reach and provides confidence in its predictive capability for flood routing and hydraulic analysis.

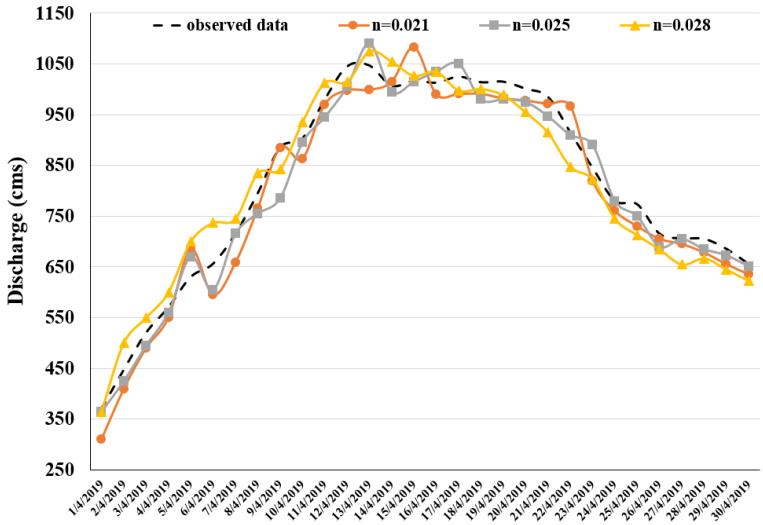

Fig. 4. Comparison of simulated and observed discharge hydrographs for the Tigris River.

4.2. Simulation of stages and discharges for different Manning's values

The HEC-RAS model simulations underscore a critical point: the model's output, specifically river flow and water levels, demonstrates significant sensitivity to adjustments in Manning's roughness coefficient. This parameter, which accounts for the frictional resistance of the channel surface, was varied within a plausible range. For the Tigris River, the 'n' values explored were between 0.021 and 0.037, while for the Al-Musandawq channel, the range was from 0.020 to 0.030. These ranges were selected based on typical values for riverine environments and were adjusted during the calibration process. It is also acknowledged that the simulations are inherently influenced by the uncertainties present in the historical hydrographic data, a common challenge in hydrological modeling.

To rigorously evaluate the model's performance and the reliability of the calibration, several key statistical indicators were employed. These metrics allow for a quantitative comparison between the simulated flow data generated by the model and the actual observed flows. The RMSE and NSE were the primary indicators selected for this performance assessment, with calculations performed assuming a daily time step (t=1 day).

4.2.1. For the Tigris river cross-section

The calibration process yielded a range of statistical results across different Manning's 'n' values. When 'n' was set to 0.021, the MAE was 33.038, the NSE was 0.964, and the RMSE was 37.358. As the 'n' value increased, the performance generally improved. The optimal 'n' value of 0.031 for the Tigris River resulted in the most favorable statistical outcomes: an MAE of 24.350, an outstanding NSE of 0.979, and an RMSE of 28.474. This high NSE value (closer to 1) signifies a very strong agreement between the simulated and observed flows, indicating that the model, with this roughness coefficient, accurately captures the river's dynamic behavior. Even with slightly higher 'n' values (0.034 and 0.037), the NSE remained strong (0.978 and 0.976, respectively), with comparable RMSE values (29.078 and 30.105), suggesting a robust performance over a narrow range of roughness coefficients. The chosen value of n = 0.031 represents the best fit, balancing accuracy with realistic parameterization (Table 2).

4.2.2. For the Al-Musandawq channel

The calibration for the Al-Musandawq channel also demonstrated excellent model performance. With an 'n' value of 0.020, the

MAE was 12.833, the NSE was 0.972, and the RMSE was 14.090. The performance metrics consistently improved as the 'n' value increased. The highest NSE value of 0.986 was achieved when Manning's 'n' was set to 0.028, accompanied by an MAE of 9.033 and an RMSE of 10.571. This exceptionally high NSE value indicates a near-perfect match between the simulated and observed flows in the Al-Musandawq channel, reflecting the model's high fidelity in representing the flow dynamics within this specific channel. The subsequent increase in 'n' to 0.030 still yielded strong results (NSE: 0.983, RMSE: 11.422), but the value of n=0.028 provided the most accurate representation (Table 3).

The comprehensive statistical evaluation unequivocally shows that setting Manning's roughness coefficient to 0.031 for the Tigris River and 0.028 for the Al-Musandawq channel yielded hydrographs that most closely align with the observed data. The reported statistical indicators, particularly the high NSE values (0.979 for the Tigris and 0.986 for the Al-Musandawq) and relatively low RMSE values, provide strong quantitative evidence of the model's accuracy and robustness. These values signify that the calibrated model is highly capable of reproducing the historical flow patterns.

Fig. 4 visually corroborates these findings by presenting the flow hydrographs for the Tigris River cross-section. The plots clearly illustrate the superior agreement between the simulated discharges (using the optimized 'n' values) and the measured discharges, providing a compelling qualitative complement to the statistical results. The visual concordance reinforces confidence in the model's calibration and its suitability for subsequent simulation tasks, such as evaluating flood management strategies.

Table 2. Statistical evaluation of calibration results for the Tigris River cross-section.

n	RMSE	NSE	MAE
0.021	37.358	0.964	33.038
0.025	34.103	0.971	27.564
0.028	32.667	0.952	30.549
0.031	28.474	0.979	24.35
0.034	29.078	0.978	25.884
0.037	30.105	0.976	24.796

Table 3. Statistical evaluation of calibration results for the Al-Musandawq channel.

n	RMSE	NSE	MAE
0.02	14.09	0.972	12.833
0.024	12.205	0.981	10.033
0.028	**10.571**	**0.986**	**9.033**
0.03	11.422	0.983	9.833

4.3. Results of one- and two-dimensional mathematical models

a) Water depth, velocity, and water surface profile

Figs. 5 to 7 illustrate the simulated hydraulic parameters along the study reach, including water depth, flow velocity, and water surface profile, as generated by the HEC-RAS model. Analysis of the model outputs indicates that flow velocities range from 0 to 2.3 m/s, with the maximum value of 2.3 m/s occurring at station 23+596. Simulated water depths vary between 0 and 7.2 m across the study reach. Accordingly, the water surface elevations at the upstream and downstream boundaries are 17.11 meters above sea level (masl). and 6.55 masl, respectively, reflecting the overall bed gradient and hydraulic conditions along the river reach.

Fig. 5. Spatial distribution of water depth corresponding to the peak flow condition.

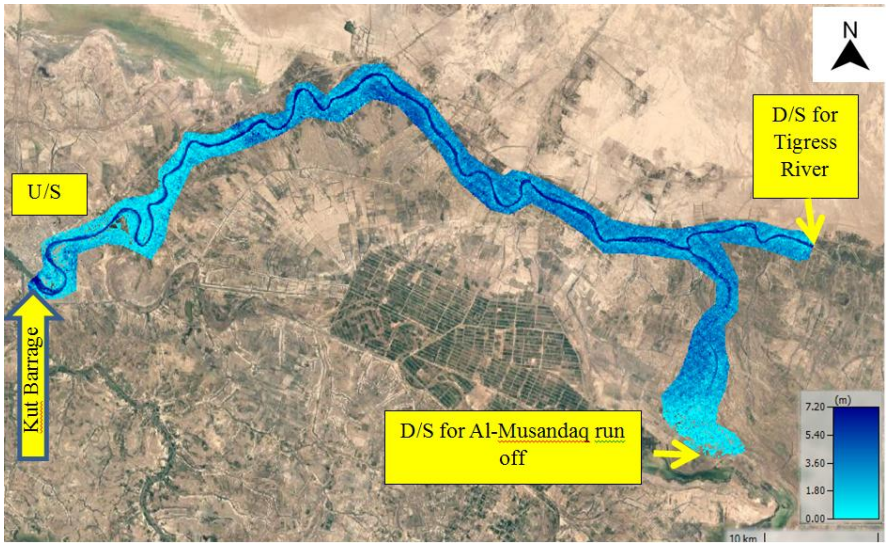

Fig. 6. Flow velocity field corresponding to the peak flow condition.

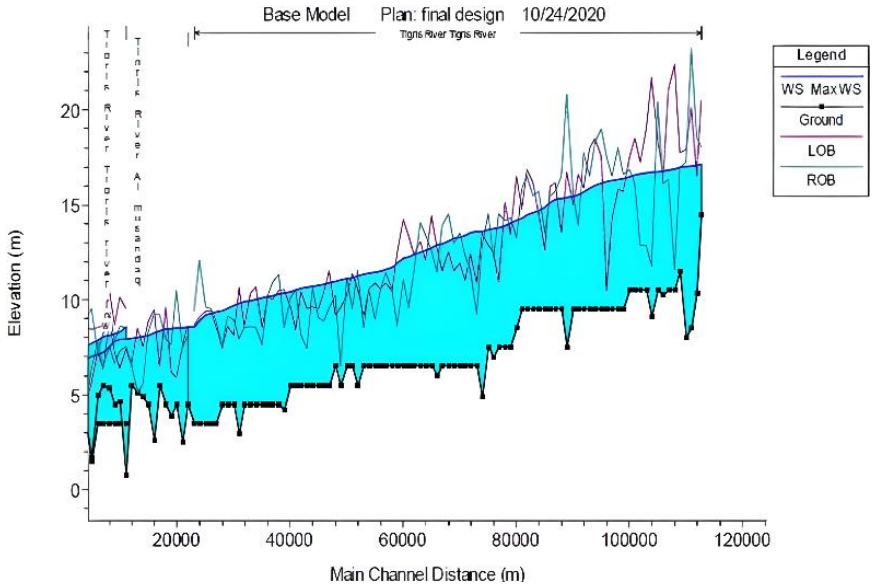

Fig. 7. Simulated water surface profile of the study reach at peak flow conditions.

4.4. Removal of islands and sidebars from the Tigris River in the study area

As noted earlier, the flood wave originating downstream of the Kut Dam propagated rapidly, reaching Maysan City within three days and causing flooding. To mitigate this risk and restore the river's capacity to convey expected flood discharges, a scenario was developed in which islands and sidebars within the river reach, from downstream of the Kut Dam to the Al-Musandawq channel, were removed. This was achieved by modifying the river cross-sections in the HEC-RAS model to reflect the absence of these features. Fig. 8 presents a satellite image of the five islands and one sidebar along the study reach of the Tigris River, highlighting their positions. The sequence and locations of these features are summarized in Table 4, providing a reference for their removal in the hydraulic simulations.

Table 4. Spatial coordinates of islands and sidebars along the study reach.

Sample	Station	Type
1	112+596	Island
2	107+596	Sidebar
3	99+596	Island
4	63+596	Island
5	34+596	Island
6	25+596	Island

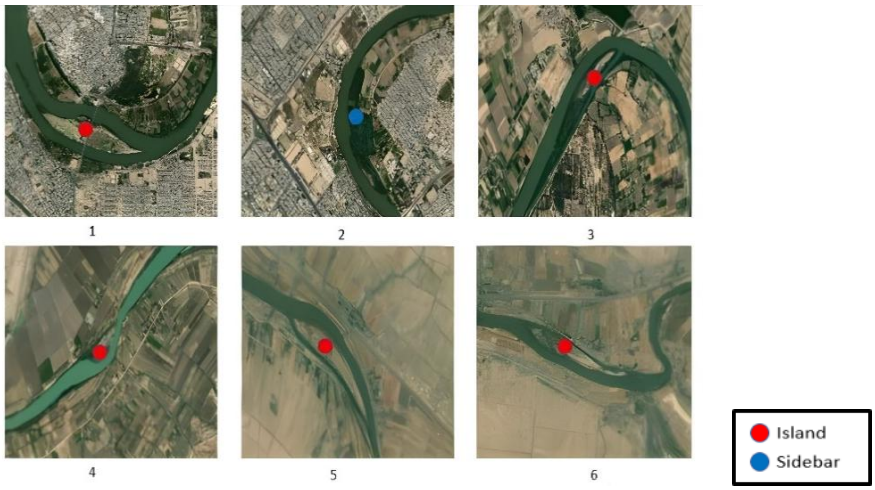

Fig. 8. Satellite imagery showing the locations of islands and a sidebar along the Tigris River study reach.

The cross-sections of the Tigris River at the identified islands and sidebars were modified by reshaping them to represent unobstructed flow paths. The resulting adjusted cross-sections are presented in Figs. 9 to 14, illustrating the hydraulic configuration after the removal of these features.

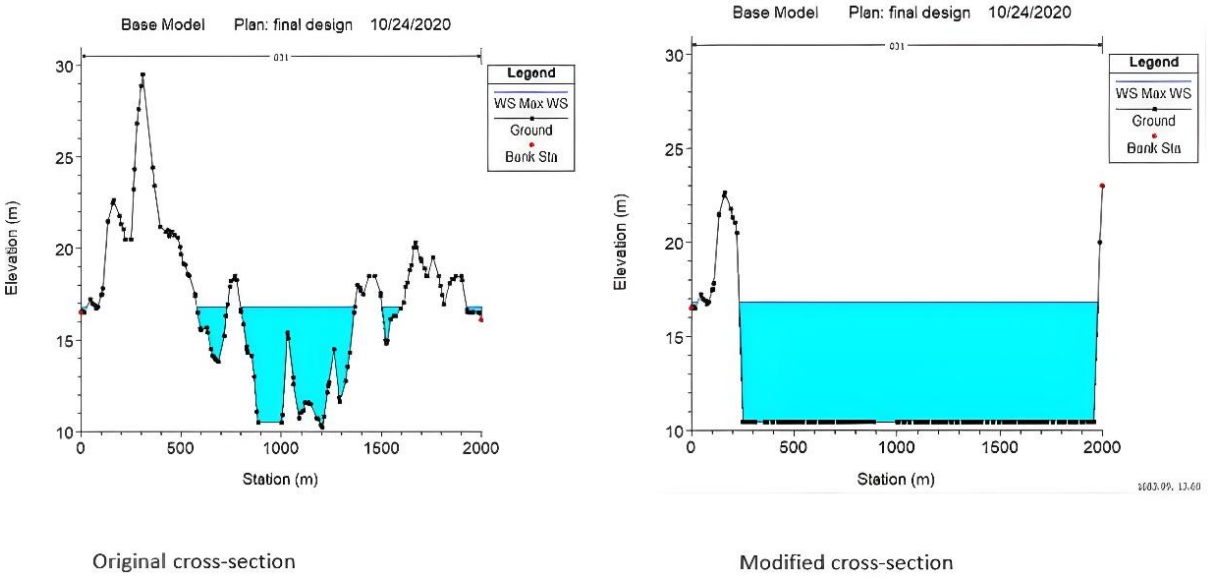

Fig. 9. Modified river cross-section at station 112+596 after removal of islands and sidebars.

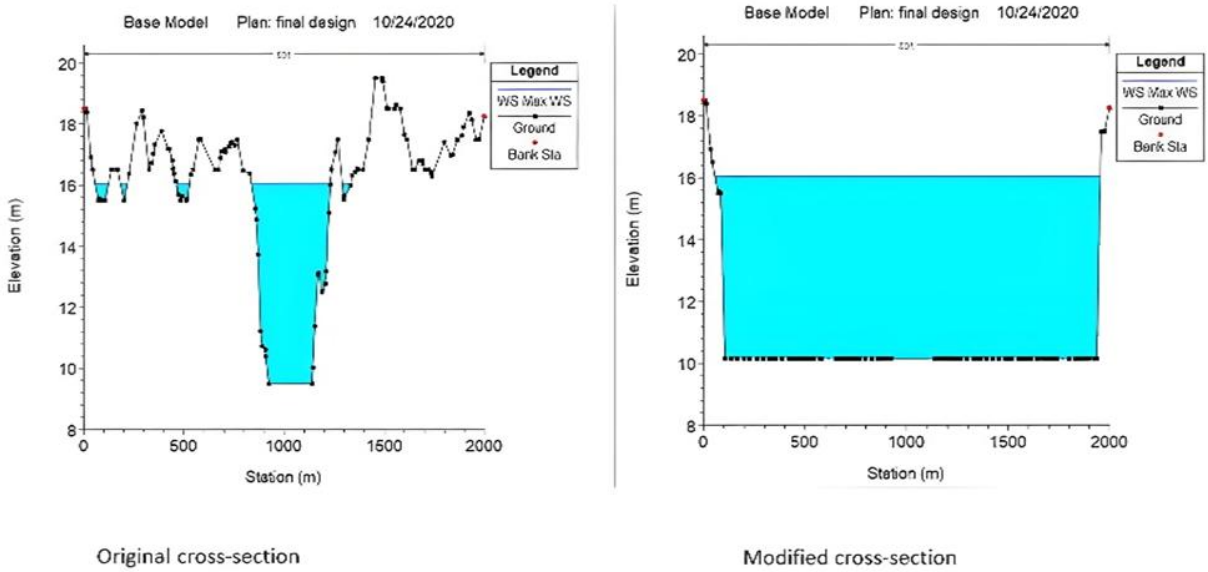

Fig. 10. Modified river cross-section at station 107+596 following the removal of islands and sidebars.

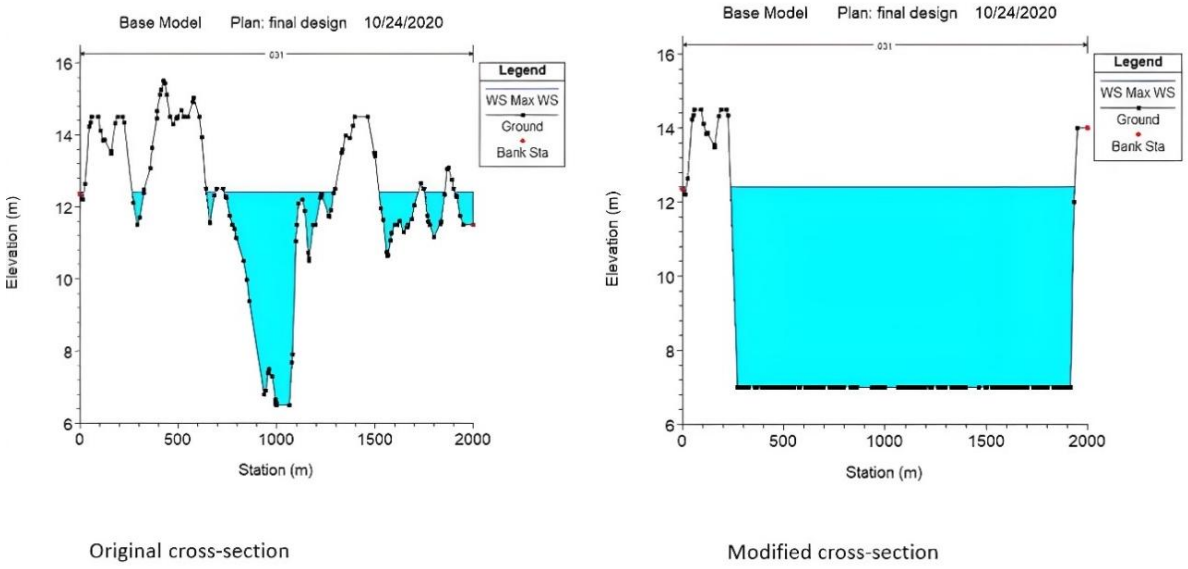

Fig. 11. Modified river cross-section at station 99+596 following the removal of islands and sidebars.

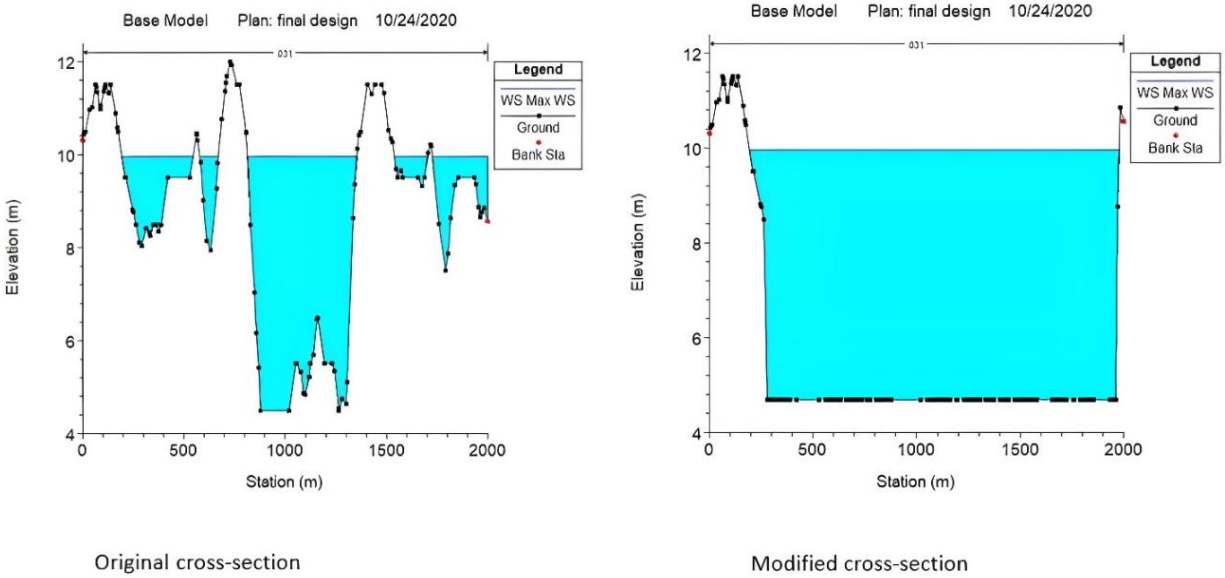

Fig. 12. Modified river cross-section at station 63+596 following the removal of islands and sidebars.

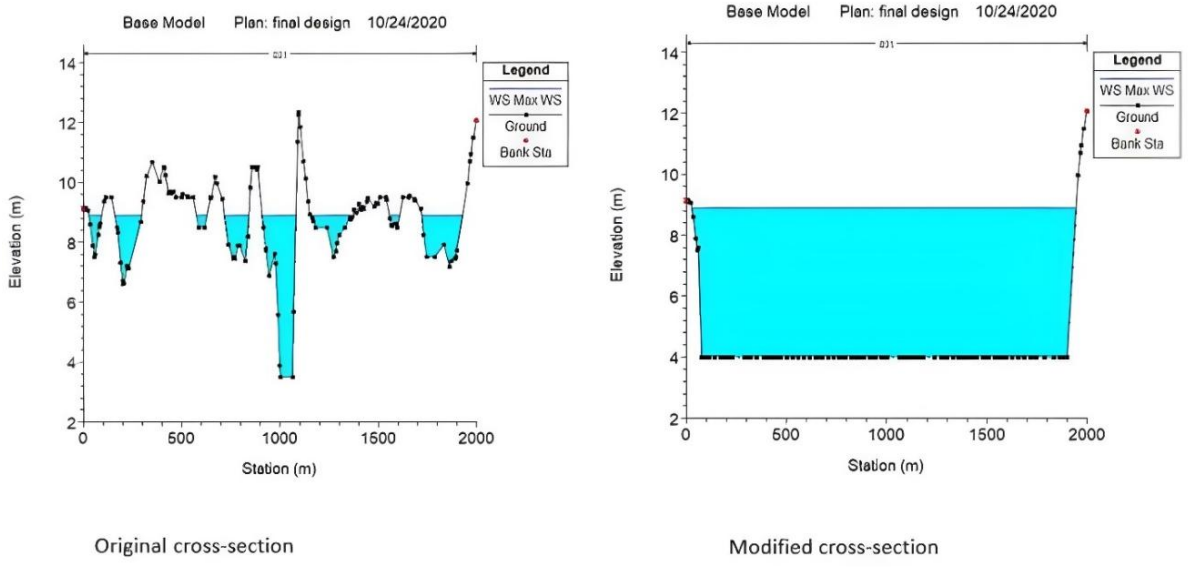

Fig. 13. Modified river cross-section at station 34+596 following the removal of islands and sidebars.

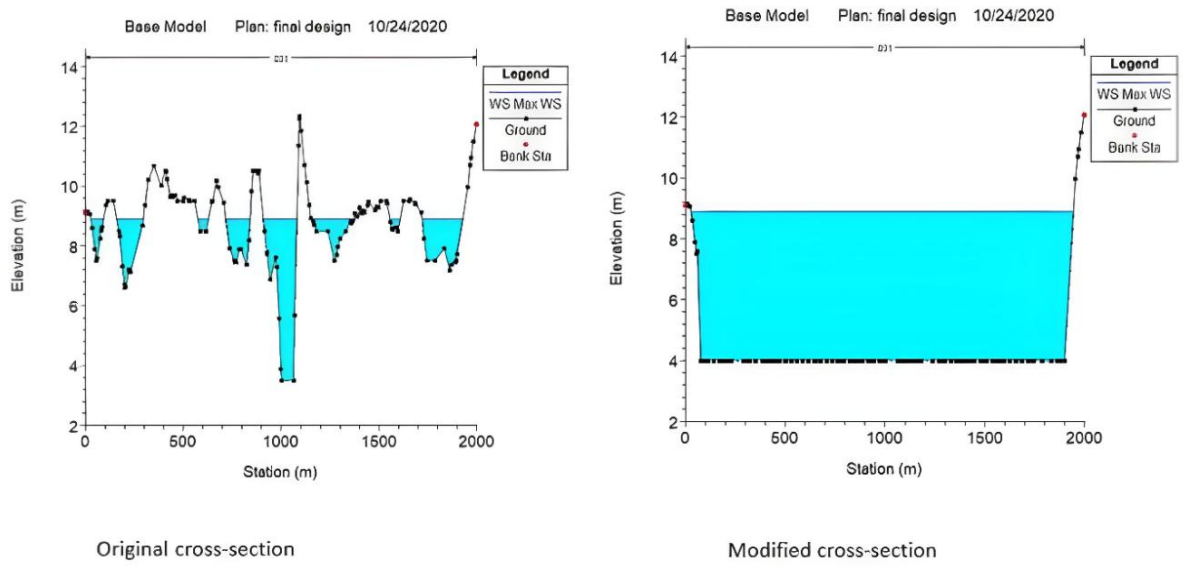

Fig. 14. Modified river cross-section at station 25+596 following the removal of islands and sidebars.

The simulation results obtained using the modified cross-sections, in which the islands and sidebars were removed (Fig. 15 and 16), indicated that the flood wave neither attenuated nor experienced a significant delay in reaching stations 114+307 and 24+596. Consequently, the strategy of physically removing islands and sidebars, or undertaking extensive river pruning and channel modifications, was deemed impractical due to its technical complexity and prohibitive cost.

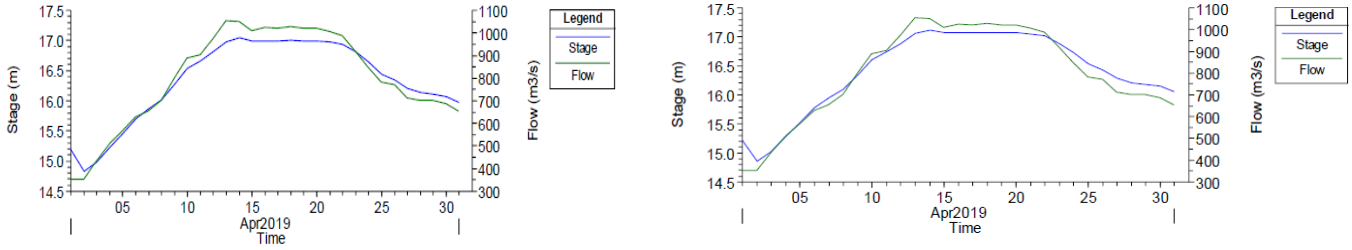

Fig. 15. Stage and flow hydrographs at Kut Barrage with (a) original cross-section and (b) modified cross-section (station 114+307).

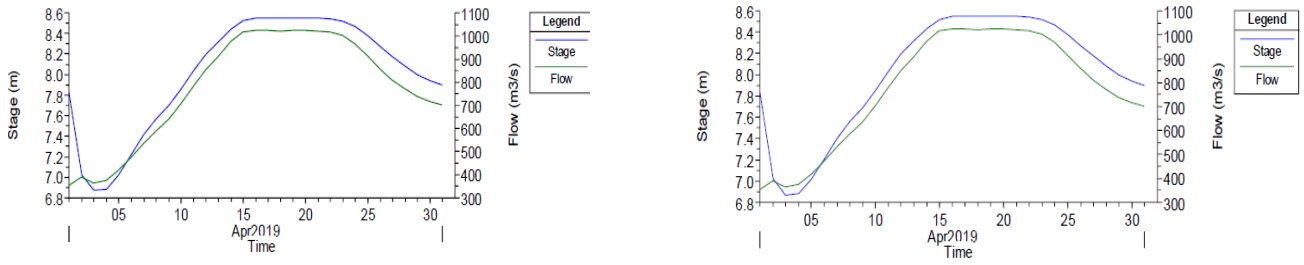

Fig. 16. Stage and flow hydrographs at the Al-Musandawq diversion point from the Tigris River with (a) original cross-section and (b) modified cross-section (station 24+596).

4.5. Design of a weir with optimal crest elevation

HEC-RAS provides multiple approaches to simulate hydraulic control structures, which include bridges, culverts, inline and lateral structures, and connections between 1D and 2D flow zones. These hydraulic controls modify the standard conservation equations applied over 1D cross-sections or 2D cells using empirically derived and typically stable formulations.

Among these, weir structures are widely used to represent flow regulation over barriers. HEC-RAS allows weir flow to be modeled in several ways, depending on the type of structure: inline weirs without gates, lateral weirs without gates, and gated weirs. Although all approaches are based on the same fundamental equations, each scenario requires specific considerations in applying the weir formulation. The discharge over a weir is calculated using Eq. 15:

$$Q = CLH^{2/3} \tag{15}$$

where, Q is the flow rate (m³/s), C is the weir coefficient, L is the crest length of the weir, and H is the energy head above the crest.

This investigation employs ungated inline weirs as a strategic approach for flood control. Specifically, a weir was implemented upstream of the Al-Musandawq channel at station 23+410, configured with a 10 m crest width and a weir coefficient of 3.1, situated 20 m from the upstream cross-section. To thoroughly assess the efficacy of this submerged weir in moderating Tigris River floods across the study reach, five distinct scenarios were devised. The overarching design objective is to regulate the flow reaching Amarah city, restricting it to 700 m³/s during peak flood seasons while ensuring a minimum passage of below 250 m³/s during drier periods.

As an illustrative example, the outcomes derived from one scenario are detailed in this section. A comprehensive presentation of the results across all five scenarios is subsequently provided in Table 7.

4.6. Scenario with peak flow of 1025 m³/s

This scenario was designed based on the maximum observed discharge of 1025 m³/s released from the Kut Dam, as recorded in the flood events of 1995 and 2019. Two sub-cases were considered for the simulation:

- **Case 1:** Lateral inflow equal to 0 m³/s
- **Case 2:** Lateral inflow equal to 525 m³/s

The corresponding hydraulic data for these scenarios are summarized in Tables 5 and 6. These simulations were used to evaluate the optimal crest elevation of the weir to ensure effective flood diversion while maintaining safe flow conditions downstream.

Table 5. Assumed lateral inflow parameters along the study reach for a total discharge of 1025 m³/s (Case 1).

Discharge in Tigris River (m^3/s)	Name of lateral inflows	Discharge (m^3/s)	Weir elevation (m)
1025	-	-	9.406
1025	Um Aljury	0	9.406
1025	Al-Chabbab	0	9.406

Based on this scenario (Case 1), the peak flow entering Maysan City is 346.29 m^3/s, while the maximum discharge directed toward the Al-Musandawq channel reaches 675.73 m³/s. The maximum water surface elevation is 8.65 m at station 23+610, located upstream of the Al-Musandawq channel, and 8.32 m at station 23+596, situated downstream of the Al-Musandawq channel.

Table 6. Assumed lateral inflow parameters along the study reach for a total discharge of 1025 m³/s (Case 2).

Discharge in Tigris River (m^3/s)	Name of lateral inflows	Discharge (m^3/s)	Weir elevation (m)
1025	-	-	9.406
1050	Um Aljury	25	9.406
1550	Al-Chabbab	500	9.406

In Case 2, the hydraulic analysis indicated that the maximum inflow rate into the Maysan city area is 389.18 m^3/s, while the maximum flow entering the Al-Musandawq channel is 1159.73 m^3/s. Specifically, the maximum water surface elevation reaches 8.71 m at station $23 + 610$ (upstream of the Al-Musandawq channel structure) and 8.41 m at station $23 + 596$ (downstream).

The simulation results, generated using historical flood data spanning from 1995 to 2019, were instrumental in pinpointing the optimal design parameters for the proposed weir. The simulations revealed that a crest elevation of 9.406 meters for the weir is the most effective in managing river discharge. This specific elevation ensures that the flow directed towards Maysan city is capped at a maximum of 700 m^3/s, thereby preventing catastrophic inundation. Simultaneously, it guarantees a minimum flow of 250 m^3/s, crucial for maintaining ecological balance and water supply during drier periods. This optimized elevation underpins the decision to implement the final flood control structure as a submerged weir precisely at 9.406 m.

The proposed structure is not merely defined by its elevation but also by its physical characteristics and strategic placement. With a crest width of 5 meters and an approximate total length of 130 meters, the weir is designed for robust performance. Its location upstream of the Al-Musandawq channel is a key design feature, allowing for the strategic diversion of excess floodwaters.

Table 7 provides a quantitative summary of the simulation outcomes across various scenarios, focusing on different discharge rates. For a peak inflow of 4000 m^3/s in the Tigris River, the weir at 9.406 m elevation successfully diverts 3322.51 m^3/s through the Al Musandawi channel while allowing only 675.62 m^3/s to pass towards Maysan. Similar effective flow management is observed for other simulated peak flows, such as 2500 m^3/s (with 1907.09 m^3/s diverted and 582.27 m^3/s to Maysan) and 1025 m^3/s (with 675.73 m^3/s diverted and 346.29 m^3/s to Maysan). The simulations demonstrate a consistent pattern: as the total discharge in the Tigris River increases, a proportionally larger volume of water is successfully managed and diverted through the Al Musandawi channel, significantly reducing the burden on the Maysan reach.

Fig. 17. visually complements these findings by presenting flood hazard maps for different river reaches under the proposed flood control strategy. The generated water depth zoning maps surrounding the Tigris River offer a compelling qualitative depiction of the results. They clearly illustrate a substantial reduction in flood risk across the studied areas. The maps effectively demonstrate how the submerged weir, by controlling and diverting flood flows, ensures the safe passage of excess water away from vulnerable zones, thereby confirming the structural approach's efficacy in managing flood events. This visual evidence strongly supports the quantitative data, highlighting the practical impact of the designed intervention in mitigating flood hazards.

Table 7. Summary of simulation outcomes across different scenarios of weir discharge rates.

Discharge in Tigris River (m^3/s)	Flow pass through Maysan (m^3/s)	Flow pass through the Al Musandaq (m^3/s)	Weir elevation (m)
4000	675.62	3322.51	9.406
2500	582.27	1907.09	9.406
1025	346.29	675.73	9.406
533	330.18	203.1	9.406
1058	371.18	686.13	9.406

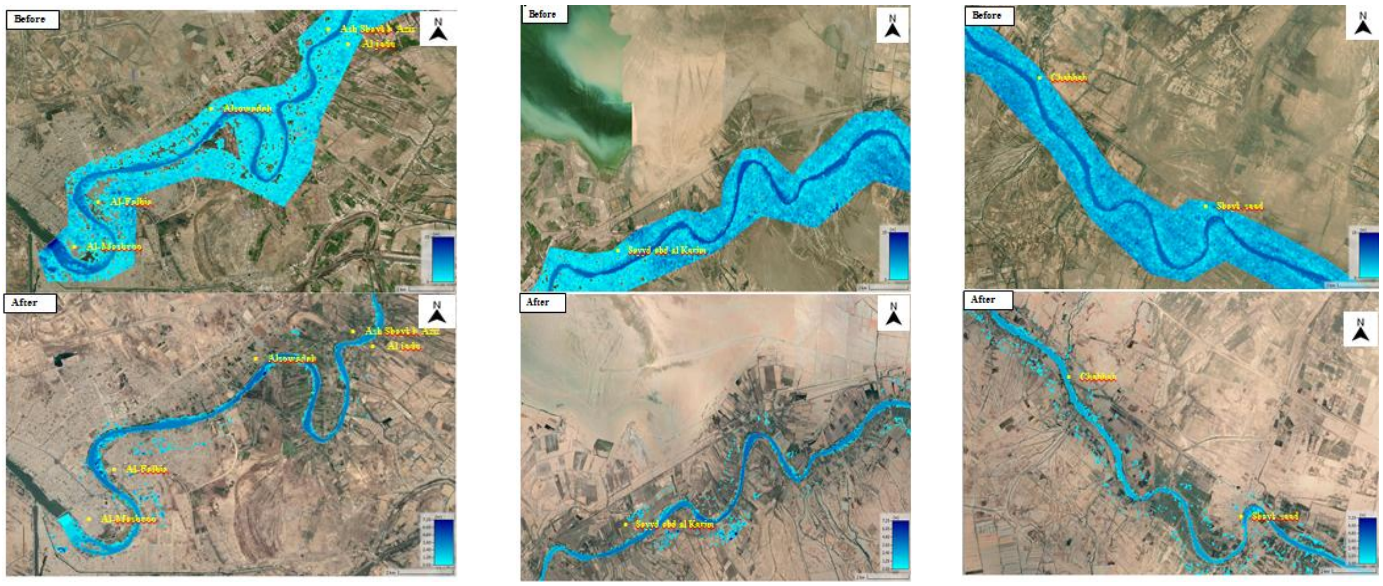

(a) (b) (c)

Fig. 17. Flood depth zoning map for before and after application of the proposed structural approach in: a) Al-Mashroo to Aziz Al-Jadu b) Sayyd Abd Al Karim c) Al-Chbbab to Shayk Saad.

4.7. Strategic policy implications and decision-making guidance

The insights derived from this research provide a foundational basis for refining water resource management and strengthening flood mitigation strategies within the Tigris River basin, with a specific focus on the vulnerability of Amarah. By successfully deploying an integrated 1D–2D HEC-RAS framework, this study underscores the model's capacity as a dependable diagnostic tool for deciphering intricate flood dynamics, even in regions characterized by data scarcity. Such an analytical approach facilitates evidence-based governance by delivering precise inundation projections and enabling a rigorous, quantitative appraisal of diverse flood control interventions. A primary takeaway for infrastructure planning is the validated efficacy of the proposed submerged weir at the Al-Musandawq channel. Specifically, maintaining an optimized crest elevation of 9.41 meters presents a technically viable structural intervention to shield Amarah from projected high-magnitude flood events. It is recommended that the Ministry of Water Resources and associated regulatory bodies integrate these technical parameters into forthcoming flood defense systems and regional developmental agendas. Moreover, the computational architecture developed herein offers a scalable blueprint for real-time early warning systems, which are essential for orchestrating timely evacuations and risk-reduction protocols. Beyond structural recommendations, this inquiry highlights the necessity of accounting for spatial heterogeneity in hydraulic variables, most notably Manning's roughness, and the complex interplay between primary riverine conduits and diversionary escape routes. Future policy frameworks should prioritize the incorporation of high-fidelity topographic datasets and sophisticated hydraulic modeling into standard management practices. Finally, while isolated natural mitigation measures showed limited success in this particular context, their evaluation points toward the imperative for a hybrid mitigation paradigm. This entails a synergistic combination of engineered structures and non-structural tactics, such as strategic land-use zoning and community-driven awareness initiatives, to achieve a holistic and resilient flood risk management posture.

5. Conclusion

This study successfully addressed the critical challenge of managing flood hazards in the Tigris River downstream of the Kut Dam, with a specific focus on protecting the city of Amarah by modeling the Al-Musandawq channel. The primary objective was to investigate flood behavior and explore effective flood management strategies within this reach. Through the development and calibration of an integrated 1D–2D HEC-RAS hydraulic model, we achieved a robust simulation of flood wave propagation for the 2019 event, applying both one-dimensional and more advanced two-dimensional modeling approaches to assess flood behavior and control. The findings confirm the critical role of advanced hydraulic modeling, particularly coupled 1D–2D approaches, in understanding complex flood dynamics and assessing mitigation alternatives in regions with limited data. This research provides

valuable insights and practical recommendations for water resource managers and policymakers in Iraq, offering a scientifically validated strategy for enhancing flood resilience in vulnerable areas. The key findings of this research are summarized as follows:

- **Calibration of Manning's Roughness Coefficient:** The optimal Manning's n values, 0.031 for the Tigris River and 0.028 for the Al-Musandawq channel, demonstrated an excellent agreement between simulated and observed flow data. The model performance metrics were robust, with MAE values of 9.033 m³/s, RMSE values of 10.57 m³/s, and NSE values of 0.986, all within acceptable ranges.
- **Effect of Island and Sidebar Removal:** Simulations indicated that the removal of all islands and sidebars along the river did not significantly dissipate the flood wave. Additionally, this approach is often considered impractical due to the technical difficulty and high cost associated with large-scale river modification.
- **Optimal Weir Design for Flood Control:** The study identified that the most effective method for managing floodwaters is the implementation of a weir with an optimal crest elevation. A barrier set at 9.4 m effectively limits peak flows to less than 700 m³/s entering Maysan City, ensures minimal flows (below 250 m³/s) during dry seasons, and allows controlled flows between 250 and 700 m³/s to pass downstream.

Based on the findings of this study, the following avenues are suggested for future work:

- **Construction of the Al-Musandawq Diversion System:** Development of an engineered system to divert water from the Tigris River into the Al-Musandawq pond in Maysan City could further enhance flood mitigation.
- **Irrigation Potential During Low Flows:** Investigate the feasibility of using the Al-Musandawq channel to supply water for agricultural or roadside irrigation during the winter months, providing a secondary benefit of managed water storage.
- Integrating the proposed model into a real-time forecasting system and exploring the long-term morphological impacts of the proposed weir.

Statements & Declarations

Author Contributions

Mahmoud Mohammad Rezapour Tabari: Conceptualization, Supervision, Methodology, investigation, editing, Formal analysis, Resources, Original Draft

Milad Rahshabdiz: Visualization, Editing

Mustafa Khudhair Tuama: Software, Visualization, writing-original draft preparation

Funding

The authors received no financial support for the research, authorship, and/or publication of this article.

Data availability

The data presented in this study will be available on request from the corresponding author.

Declarations

The authors declare no conflict of interest.

References

[1] Aerts, J. C., Botzen, W. W. Climate change impacts on pricing long-term flood insurance: A comprehensive study for the Netherlands. Global environmental change, 2011; 21: 1045–1060. doi:10.1016/j.gloenvcha.2011.04.005.

[2] Mohammed-Ali, W. S., Khairallah, R. S. Flood Risk Analysis: The Case of Tigris River (Tikrit/Iraq). Tikrit Journal of Engineering Sciences, 2023; 30: 112–118. doi:10.25130/tjes.30.1.11.

[3] Sabeeh, N. N., Alabdraba, W. M. S. The Hydrodynamic Model using HEC-RAS: The case of Tigris River Downstream of Samarra Barrage (Iraq). In: InIOP Conference Series: Earth and Environmental Science; 2022; p. 012017.

[4] Pekel, J. F., Cottam, A., Gorelick, N., Belward, A. S. High-resolution mapping of global surface water and its long-term changes. Nature, 2016; 540: 418–422. doi:10.1038/nature20584.

[5] Yarahmadi, M., Eskandari Damaneh, H., Khalighi Sigaroodi, S. Assessment of the Impact of Land Use/Land Cover Changes in the Hamoun Wetland on Land Surface Temperature Using Satellite Imagery. Civil Engineering and Applied Solutions, 2025; 1: 31–42. doi:10.22080/ceas.2025.29153.1009.

[6] Tellman, B., Sullivan, J. A., Kuhn, C., Kettner, A. J., Doyle, C. S., Brakenridge, G. R., Erickson, T. A., Slayback, D. A. Satellite imaging reveals increased proportion of population exposed to floods. Nature, 2021; 596: 80–86. doi:10.1038/s41586-021-03695-w.

[7] Nearing, G., Cohen, D., Dube, V., Gauch, M., Gilon, O., Harrigan, S., Hassidim, A., Klotz, D., Kratzert, F., Metzger, A., Nevo, S. Global prediction of extreme floods in ungauged watersheds. Nature, 2024; 627: 559–563. doi:10.1038/s41586-024-07145-1.

[8] Suresh, S., Hossain, F., Minocha, S., Das, P., Khan, S., Lee, H., Andreadis, K., Oddo, P. Satellite-based tracking of reservoir operations for flood management during the 2018 extreme weather event in Kerala, India. Remote Sensing of Environment, 2024; 307: 114149. doi:10.1016/j.rse.2024.114149.

[9] Aziz, F., Wang, X., Mahmood, M. Q., Awais, M., Trenouth, B. Coastal urban flood risk management: Challenges and opportunities− A systematic review. Journal of Hydrology, 2024; 645: 132271. doi:10.1016/j.jhydrol.2024.132271.

[10] Hansson, K., Danielson, M., Ekenberg, L. A framework for evaluation of flood management strategies. Journal of environmental management, 2008; 86: 465–480. doi:10.1016/j.jenvman.2006.12.037.

[11] Menoni, S., Molinari, D., Ballio, F., Minucci, G., Mejri, O., Atun, F., Berni, N., Pandolfo, C. Flood damage: a model for consistent, complete and multipurpose scenarios. Natural Hazards and Earth System Sciences, 2016; 16: 2783–2797. doi:10.5194/nhess-16-2783-2016.

[12] Hino, M., BenDor, T. K., Branham, J., Kaza, N., Sebastian, A., Sweeney, S. Growing safely or building risk? Journal of the American Planning Association, 2024; 90: 50–62. doi:10.1080/01944363.2022.2141821.

[13] Chakraborty, L., Thistlethwaite, J., Scott, D., Henstra, D., Minano, A., Rus, H. Assessing social vulnerability and identifying spatial hotspots of flood risk to inform socially just flood management policy. Risk Analysis, 2023; 43: 1058–1078. doi:10.1111/risa.13978.

[14] Jemberie, M. A., Melesse, A. M. Urban flood management through urban land use optimization using LID techniques, city of Addis Ababa, Ethiopia. Water, 2021; 13: 1721. doi:10.3390/w13131721.

[15] Long'or Lokidor, P., Taka, M., Lashford, C., Charlesworth, S. Nature-based solutions for sustainable flood management in East Africa. Journal of Flood Risk Management, 2024; 17: e12954. doi:10.1111/jfr3.12954.

[16] Erena, S. H., Worku, H., De Paola, F. Flood hazard mapping using FLO-2D and local management strategies of Dire Dawa city, Ethiopia. Journal of Hydrology: Regional Studies, 2018; 19: 224–239. doi:10.1016/j.ejrh.2018.09.005.

[17] Nigusse, A. G., Adhanom, O. G. Flood hazard and flood risk vulnerability mapping using geo-spatial and MCDA around Adigrat, Tigray region, Northern Ethiopia. Momona Ethiopian Journal of Science, 2019; 11: 90–107. doi:10.4314/mejs.v11i1.6.

[18] Ban, H. J., Kwon, Y. J., Shin, H., Ryu, H. S., Hong, S. Flood monitoring using satellite-based RGB composite imagery and refractive index retrieval in visible and near-infrared bands. Remote Sensing, 2017; 9: 313. doi:10.3390/rs9040313.

[19] Ruiz-Bellet, J. L., Balasch, J. C., Tuset, J., Barriendos, M., Mazon, J., Pino, D. Historical, hydraulic, hydrological and meteorological reconstruction of Santa Tecla flash floods in Catalonia (NE Iberian Peninsula). Journal of Hydrology, 2015; 524: 279–295. doi:10.1016/j.jhydrol.2015.02.023.

[20] Chaudhry, M. H. Applied hydraulic transients. 3 ed. New York (US): Springer; 2014. doi:10.1007/978-1-4614-8538-4.

[21] Brunner, G. W. HEC-RAS river analysis system 2D modeling user's manual. US Army Corps of Engineers—Hydrologic Engineering Center. 2016. Report No.:

[22] Babister, M., Barton, C. Australian Rainfall and Runoff Revision Project 15: Two Dimensional Modelling in Urban and Rural Floodplains. Canberra (AUS): Geoscience; 2012. Report No.: P15/S1/009.

[23] Maidment, D. R., Mays, L. W. Applied hydrology, Water Resources Handbook. Applied hydrology, Water Resources Handbook. New York, NY, USA: McGraw-Hill. ed. 1988.

[24] Chow, V. T. Open Channel Hydraulics. Il ed. Mc Graw Hill, New York; 1950.